Implementation of an experimentally feasible controlled-phase gate on two blockaded Rydberg atoms

Matthias M. Müller,* Michael Murphy, Simone Montangero, and Tommaso Calarco
Institut für Quanteninformationsverarbeitung, Universität Ulm, Albert-Einstein-Allee 11, D-89069 Ulm, Germany

Philippe Grangier and Antoine Browaeys
Laboratoire Charles Fabry, Institut d'Optique, CNRS, Université Paris-Sud, Campus Polytechnique, RD 128, 91127 Palaiseau Cedex, France
(Received 28 October 2013; published 28 March 2014)

We investigate the implementation of a controlled-Z gate on a pair of Rydberg atoms in spatially separated dipole traps where the joint excitation of both atoms into the Rydberg level is strongly suppressed (the Rydberg blockade). We follow the adiabatic gate scheme of Jaksch *et al.* [D. Jaksch, J. I. Cirac, P. Zoller, S. L. Rolston, R. Côté, and M. D. Lukin, Phys. Rev. Lett. **85**, 2208 (2000)], where the pair of atoms is coherently excited using lasers, and apply it to the experimental setup outlined by Gaëtan *et al.* [A. Gaëtan, Y. Miroshnychenko, T. Wilk, A. Chotia, M. Viteau, D. Comparat, P. Pillet, A. Browaeys, and P. Grangier, Nat. Phys. **5**, 115 (2009)]. We apply optimization to the experimental parameters to improve gate fidelity and consider the impact of several experimental constraints on the gate success.

DOI: 10.1103/PhysRevA.89.032334 PACS number(s): 03.67.Ac, 32.80.Rm

I. INTRODUCTION

Using neutral atoms for quantum information has garnered much theoretical interest over the last decade, fueled by advances in their experimental manipulation, particularly trapping and cooling. Several schemes for entangling pairs of atoms (an essential operation for quantum logic) via controlled collisions have been developed [1,2], but schemes that make use of the special properties of Rydberg atoms are also very promising (see Ref. [3] for a review). In particular, several schemes for producing quantum gates by exciting pairs of Rydberg atoms with tuned lasers have emerged [4,5] which capitalize on the strong dipole-dipole interaction that prevents the simultaneous excitation of neighboring Rydberg atoms, known as the Rydberg blockade. Several steps towards realizing such schemes experimentally have already been achieved, particularly the observation of the blockade [6] and entanglement generation [7] in a system of two confined Rydberg atoms. There has even been some early success in producing a gate with trapped Rydberg atoms [8].

In this paper, we consider the implementation of a controlled-Z (CZ) gate on a pair of Rydberg atoms confined in spatially separated dipole traps subject to the Rydberg blockade effect. We follow the scheme outlined in Ref. [4], but with specific application to the experimental setup detailed in Ref. [9], where the Rydberg atom is excited via a two-photon transition. This proposal has the advantage that both atoms are excited by the same laser, reducing the need for single-atom addressability; the gate is also adiabatic, which softens the experimental requirement for strong fields or precise timings. However, the experimental considerations do present additional challenges in the implementation of the gate, particularly due to loss from the intermediate state of the transition and the movement of the atoms in the dipole trap. We attempt to address both of these issues here by applying a direct search control algorithm to search for the ideal set of parameters for implementing the gate on a short timescale ($\sim 1\ \mu$s) and with high fidelity. Our results show that the physical system allows for a great deal of control and gate times and fidelities approaching our desired range, providing a positive outlook for implementing high-fidelity gates with such systems.

The paper is arranged as follows. In Sec. II, we briefly recount the CZ gate, followed by a description of how it may be synthesized on a pair of Rydberg atoms. In particular, we expose the operation of the gate by considering the effective two-level dynamics of each atom and its interaction with a laser field. In Sec. III, we describe how we optimize the operation of the laser using a gradient descent to achieve the gate with high fidelity. In Sec. IV, we consider the details of the experiment and the constraints it imposes on the gate operation, particularly with regards to loss and effects arising from atomic motion. Finally, we conclude our paper in Sec. V.

II. CONTROLLED-PHASE GATE

A. Gate definition

The controlled-Z (CZ) gate is a two-qubit gate in quantum information and belongs to the class of controlled unitary operations [10]. Given the computational basis $|0\rangle, |1\rangle$, it is defined as the unitary transformation

$$\mathrm{CZ} = \begin{pmatrix} 1 & 0 & 0 & 0 \\ 0 & 1 & 0 & 0 \\ 0 & 0 & 1 & 0 \\ 0 & 0 & 0 & -1 \end{pmatrix}. \tag{1}$$

This gate is of particular importance because it can generate entanglement between two unentangled qubits depending on the initial states of the qubits. In addition, together with a finite set of single-qubit operations, one can construct any desired gate operation simply by taking combinations of these operations with the CZ gate. This is known as a universal set for quantum computation [11].

*matthias.m.mueller@uni-ulm.de

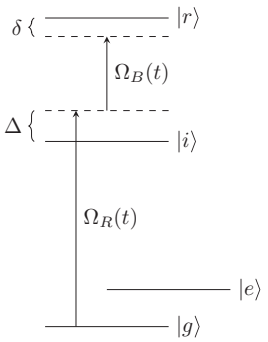

FIG. 1. The level scheme for a single Rydberg atom. The atom is driven to the Rydberg state via a two-photon transition, which couples the ground state $|g\rangle$ to the excited state $|r\rangle$ through the intermediate state $|i\rangle$. The effective Rabi frequencies of the transitions are $\Omega_R(t)$ for the red laser (which is blue-detuned by Δ) and Ω_B for the blue laser (which is red-detuned by $\Delta + \delta$).

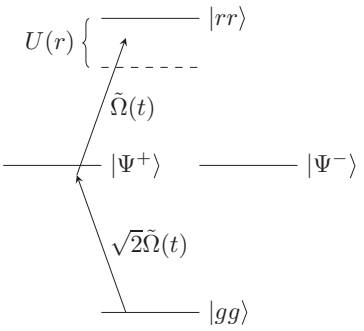

FIG. 2. The level scheme for the two-atom system (neglecting the internal level $|i\rangle$). The transition from the joint ground state $|gg\rangle$ to the super-radiant state $|\Psi^+\rangle = (|gr\rangle + |rg\rangle)/\sqrt{2}$ is enhanced by a factor of $\sqrt{2}$, while there is no coupling to the subradiant $|\Psi^-\rangle = (|gr\rangle - |rg\rangle)/\sqrt{2}$ state. The excitation of both atoms to the Rydberg state $|rr\rangle$ is forbidden, since the interaction energy $U(r)$ has shifted the level far off-resonant with the incident lasers.

B. Blockaded Rydberg atoms

The physical system we are considering for the implementation of the gate is a pair of trapped Rydberg atoms [6], specifically ^{87}Rb. The atoms are trapped a distance r apart in two separate microscopic dipole traps [6]. For our purposes, we need only consider a small number of the internal states on which the dynamics take place.

A pair of hyperfine states of the atom encode the computational basis and are labeled $|e\rangle = |0\rangle$, $|g\rangle = |1\rangle$. Each atom has its $|g\rangle$ state coupled to a highly excited Rydberg state (which we label $|r\rangle$) via a two-photon transition through an intermediate state $|i\rangle$. The internal level scheme with state transitions for a single atom is shown in Fig. 1. If two neighboring atoms are excited to the $|r\rangle$ state, then they interact. For the work presented we have taken a dipole-dipole potential with energy $U(r) = C_3/r^3$. However, the conclusion of the work is independent of this functional form and only the strength of the interaction at a given fixed distance of the two atoms is relevant. As a consequence our conclusions are valid also for a van der Waals interaction. The interaction energy shifts the energy of the state where both atoms are excited. When this shift is much larger than the two-photon detuning δ, the two-photon transition is far off-resonant with the doubly excited state, leading to a strong suppression of both atoms becoming excited. This effect is known as the Rydberg blockade and has been observed experimentally [6,12]. The effect is shown schematically in Fig. 2.

The important point about the blockade mechanism in our case is that it is state dependent: only if both atoms are in the ground state $|g\rangle$ will they be subject to the blockade. The potential use of this as a mechanism for performing a quantum gate has been explored in several papers [4,5,13,14], also with Krotov pulse shape optimization [15,16], but here we follow the adiabatic (model B) scheme of Jaksch *et al.*, where the gate is performed by adiabatically driving the two-atom system [4].

C. Gate operation in outline

There are two critical elements that allow us to synthesize the gate with our system. The first is the blockade mechanism, which prevents excitation to the doubly excited $|rr\rangle$ state (where we have used the shorthand notation $|r\rangle \otimes |r\rangle = |rr\rangle$ for the tensor product of the state of the two atoms, which is used throughout). This avoids unwanted mechanical effects stemming from the strong interaction of the two Rydberg atoms, as well as reducing the time spent in the Rydberg state, which is subject to loss. The second crucial aspect is the super-radiant enhancement of excitation from $|gg\rangle$ as compared with the states $|ge\rangle$ and $|eg\rangle$. In other words the Rabi frequency of this transition is enhanced by a factor $\sqrt{2}$; see Fig. 2. This results in a higher rate of phase accumulation on the $|gg\rangle$ state during excitation in comparison to $|ge\rangle$ and $|eg\rangle$. By carefully choosing the excitation profile of the incident lasers, we can control these two different accumulated phases to produce the CZ gate.

D. Hamiltonian

The two-photon transition is driven via two lasers: one blue-detuned on the transition from $|g\rangle$ to $|i\rangle$ by an amount Δ with a Rabi frequency $\Omega_R(t)$, and the other red-detuned on the transition $|i\rangle$ to $|r\rangle$ by an amount $\Delta + \delta$ with a Rabi frequency Ω_B (see Fig. 1). In addition there is loss from the states $|i\rangle$ and $|r\rangle$. The general form of the effective Hamiltonian for our two-atom system can be written as

$$\hat{H} = \hat{H}_r^1 + \hat{H}_r^2 + \hat{H}_{\text{int}}. \tag{2}$$

The single-atom Hamiltonians are composed of both the internal and external dynamics, such that (after the rotating-wave approximation)

$$\hat{H}_r^j = \hat{H}_S^j + \hat{H}_I^j + \hat{H}_E^j, \tag{3}$$

$$\hat{H}_S^j = (\Delta - i\gamma_i)|i\rangle\langle i| + (\delta - i\gamma_r)|r\rangle\langle r|, \tag{4}$$

$$\hat{H}_I^j = -\frac{\hbar\Omega_R(t)}{2} e^{i\mathbf{k_R}\cdot\mathbf{r}_j}|g\rangle\langle i| - \frac{\hbar\Omega_B}{2} e^{i\mathbf{k_B}\cdot\mathbf{r}_j}|i\rangle\langle r| + \text{H.c.}, \tag{5}$$

$$\hat{H}_E^j = (\hat{T} + V_{\text{trap}})(|g\rangle\langle g| + |e\rangle\langle e| + |i\rangle\langle i| + |r\rangle\langle r|), \tag{6}$$

where $i = 1,2$ labels the two atoms. $\hat{H}_S$ describes the energy splitting of the internal states along with the effective decay from those states. This description of the loss is valid for small loss, which is the case for the optimized version of our gates. (It is a bad description in the unoptimized cases with low fidelity and high loss, but this does not affect the results in this paper.) $\hat{H}_I$ describes the laser coupling between the internal states, and $\hat{H}_E$ contains the kinetic and potential energy terms. The factors γ_i, γ_r account for an effective loss of population from the intermediate and Rydberg levels, respectively. The exponential terms in Eq. (5) are phases accumulated by the atoms as they move through the light field of the laser; $\mathbf{k_R}$ and $\mathbf{k_B}$ are the wave vectors of the red and blue laser fields, $\mathbf{k} = \mathbf{k_R} + \mathbf{k_B}$ is the wave vector of the effective two-photon transition, and $\mathbf{r}_j$ is the position vector of the jth atom. The interaction Hamiltonian is given simply by the dipole-dipole interaction: $\hat{H}_{\text{int}} = U(r)|rr\rangle\langle rr|$.

Note that in Eq. (6) we have neglected the difference in the trapping potentials for the different internal states (in any case we turn off the trap when the gate is performed). Since there are no state-dependent terms in Eq. (6), we can neglect it in our treatment.

E. Effective two-level system dynamics

By performing an adiabatic elimination [17] of the state $|i\rangle$, we can examine the effective three-level dynamics of the system. This leads to the condition that $\Omega_R(t), \Omega_R, \delta \ll \Delta$. In addition, we make a change of basis in the subspace span$\{|gr\rangle, |rg\rangle\}$ such that the new basis vectors in this subspace are

$$|\Psi^+\rangle \equiv \frac{1}{\sqrt{2}}(e^{i\mathbf{k}\cdot\mathbf{r}_1}|gr\rangle + e^{i\mathbf{k}\cdot\mathbf{r}_2}|rg\rangle),$$
$$|\Psi^-\rangle \equiv \frac{1}{\sqrt{2}}(e^{i\mathbf{k}\cdot\mathbf{r}_1}|gr\rangle - e^{i\mathbf{k}\cdot\mathbf{r}_2}|rg\rangle). \tag{7}$$

We can now rewrite the system Hamiltonian as $\tilde{H} = \hat{H}_R + \hat{H}_{\text{int}}$, where

$$\hat{H}_R = \tilde{H}_r^1 + \tilde{H}_r^2 + \tilde{H}_I, \tag{8}$$

$$\tilde{H}_r^j = -\frac{\hbar\Omega_R^2(t)}{4\Delta}|g\rangle\langle g| + \left(\delta - \frac{\hbar\Omega_B^2}{4\Delta} - i\gamma_r\right)|r\rangle\langle r|, \tag{9}$$

$$\tilde{H}_I = -\frac{\hbar\tilde{\Omega}(t)}{2}(e^{-i\mathbf{k}\cdot\mathbf{r}_1}|ge\rangle\langle re| + e^{-i\mathbf{k}\cdot\mathbf{r}_2}|eg\rangle\langle er| + \text{H.c.})$$
$$-\sqrt{2}\,\frac{\hbar\tilde{\Omega}(t)}{2}(|gg\rangle\langle\Psi^+| + |\Psi^+\rangle\langle gg|), \tag{10}$$

with the effective Rabi frequency of the two-level dynamics

$$\tilde{\Omega}(t) = \Omega_B\Omega_R(t)/2\Delta. \tag{11}$$

The magnitude of the dipole matrix elements

$$|\langle gg|\hat{H}_I|\psi^+\rangle| = \sqrt{2}\frac{\hbar\tilde{\Omega}}{2}, \quad |\langle gg|\hat{H}_I|\psi^-\rangle| = 0,$$
$$|\langle ge|\hat{H}_I|re\rangle| = |\langle eg|\hat{H}_I|er\rangle| = \frac{\hbar\tilde{\Omega}}{2}$$

show that the state $|\Psi^-\rangle$ is not coupled to any of the other states via the laser interaction; in other words, it is subradiant [18]. In addition, the state $|\Psi^+\rangle$ is a super-radiant state, so that the coupling between the ground state $|gg\rangle$ and $|\Psi^+\rangle$ is enhanced by a factor of $\sqrt{2}$ compared to the transition $|ge\rangle \to |re\rangle$ ($|eg\rangle \to |er\rangle$).

Finally, note that since $|i\rangle$ is never populated in this approximation, we neglect the loss term γ_i. We also for the moment assume that the atoms are stationary, and so the phases accumulated from their movement in the light field can be neglected.

F. Gate operation in full

Now we describe the operation of the gate in more detail. We start with the initial state

$$|\psi(t=0)\rangle = \tfrac{1}{2}(|gg\rangle + |ge\rangle + |eg\rangle + |ee\rangle) \tag{12}$$

and define the target state at final time T,

$$|\psi_G\rangle = \tfrac{1}{2}(-|gg\rangle + |ge\rangle + |eg\rangle + |ee\rangle). \tag{13}$$

Note that while this seems to be a specific state transformation, as opposed to the unitary transformation from Eq. (1), they are in this case equivalent by virtue of the basis states $\{|gg\rangle, |ge\rangle, |eg\rangle, |ee\rangle\}$ not being directly coupled to one another. Hence any initial state-dependent phases will not affect the final outcome of the gate.

To perform the gate, the blue laser is always switched on, while the red laser is modulated in a time-dependent fashion using an acousto-optic modulator. If this modulation is slow on the timescale given by $\tilde{\Omega}(t)$ and δ, then the system will adiabatically follow the dressed states of the Hamiltonian $\tilde{H}$. Performing the same treatment as in Ref. [4] for our system, we similarly find that the energy of the dressed levels adiabatically connected to $|gg\rangle$ and $|ge\rangle$ ($|eg\rangle$) are

$$\varepsilon_{gg}(t) = \tfrac{1}{2}[\delta'' - 4E_R(t) + (\delta''^2 + 2\tilde{\Omega}^2(t))^{\frac{1}{2}}], \tag{14}$$

$$\varepsilon_{ge}(t) = \tfrac{1}{2}[\delta' - 2E_R(t) + (\delta'^2 + \tilde{\Omega}^2(t))^{\frac{1}{2}}], \tag{15}$$

respectively, where $\delta' \equiv \delta - E_B + E_R(t)$ is the effective two-photon detuning including the Stark shifts from the adiabatic elimination of $|i\rangle$:

$$E_R(t) \equiv \frac{\Omega_R^2(t)}{4\Delta}, \quad E_B \equiv \frac{\Omega_B^2}{4\Delta}; \tag{16}$$

and

$$\delta'' \equiv \delta' - \frac{\tilde{\Omega}^2(t)}{2u + 4\delta' - 4E_R(t)} \tag{17}$$

includes the additional Stark shift from the adiabatic elimination of the $|rr\rangle$ state. The final state is

$$|\psi(T)\rangle = e^{-i\phi_{gg}}|gg\rangle + e^{-i\phi_{ge}}(|ge\rangle + |eg\rangle) + |ee\rangle, \tag{18}$$

where

$$\phi_{gg} = \int_0^T \varepsilon_{gg}(t)dt, \quad \phi_{ge} = \int_0^T \varepsilon_{ge}(t)dt. \tag{19}$$

By performing state-selective qubit operations, we can realize the CZ gate. To see this, we first apply a state-selective phase on the first atom: if the first atom is in the state $|g\rangle$, then it receives a phase $e^{-i\varepsilon_{ge}}$. Similarly, we then apply the same phase

rotation on the second atom. After these operations, the state becomes

$$|\tilde{\psi}(T)\rangle = e^{-i(\phi_{gg}-2\phi_{ge})}|gg\rangle + |ge\rangle + |eg\rangle + |ee\rangle. \quad (20)$$

We can now define the gate phase

$$\phi \equiv \phi_{gg} - 2\phi_{ge}. \quad (21)$$

The operation of the gate is now clear: we seek to modulate $\Omega_R(t)$ such that $\phi = (2k+1)\pi$, $k \in \mathbb{Z}$, and there is no remaining population in the excited states of either atom (this is taken for granted in the adiabatic limit). The next step is to design $\Omega_R(t)$ to achieve these conditions.

III. OPTIMIZATION OF THE GATE

A. Simulation

The system evolves in accordance with the Schrödinger equation ($\hbar = 1$):

$$i\frac{\partial}{\partial t}|\psi(t)\rangle = \tilde{H}|\psi(t)\rangle. \quad (22)$$

Since the Hilbert space dimension $|\tilde{H}| = N$ is relatively small, we can simulate the gate by directly diagonalizing the Hamiltonian and using discrete time steps dt, such that the solution of Eq. (22) can be written as

$$|\psi(t)\rangle = Pe^{-iDdt}P^{-1}|\psi(t-dt)\rangle, \quad (23)$$

where $P = [x_1, x_2, \ldots, x_N]$ is the square matrix constructed from the eigenvectors $\mathbf{x}_i$ of $\tilde{H}$, and $D = \mathrm{diag}(\lambda_1, \lambda_2, \ldots, \lambda_N)$ is a diagonal matrix whose elements are the eigenvalues λ_i of $\tilde{H}$.

B. Optimization method

Many tools exist for numerical optimization that we could employ here to design the Rabi frequency $\Omega_R(t)$ that produces the gate. We start by making a guess for the form of $\Omega_R(t)$, so that the evolution is characterized by only a handful of parameters. One particular choice is a Gaussian:

$$\Omega_R(t) = \Omega_0\, e^{-\left(\frac{t}{\tau}\right)^2}, \quad (24)$$

where we choose $\tau = 0.2T$, with total gate operation time T. The constant Ω_0 is a parameter which we can, in principle, choose arbitrarily (in reality there are constraints on this value, which we come to later). There are also parameters associated with the system that one may vary, namely the atom separation r, the Rabi frequency Ω_B, and the detunings δ and Δ. We begin by choosing a set of reasonable values, and then we numerically optimize each of the parameters to achieve the desired gate with a high fidelity. The numerical method used to optimize the parameters is gradient descent.

As an example, we start with the set of parameters in Table I. The total time for the gate is fixed at $T = 500$ ns, and the detuning $\delta = 0$. The interaction strength is chosen as $U = 118$ GHz, corresponding to a separation of the atoms at a distance of 0.3 μm, when assuming dipole-dipole interaction $U(r) = 3200\ \mathrm{MHz}/r^3$ as in Ref. [6] was still valid at this small distance. This is a particularly strong interaction due to the existence of a Förster resonance [19,20], a point which we come back to later when we describe the experimental setup in more detail. But again only the value of the interactions enters the simulations, not the distance dependency. We define the fidelity of the gate operation as $F = |\langle\psi(T)|\psi_G\rangle|^2$. The resultant fidelity of the gate with these initial parameters is only around 89%. Now we apply our optimization algorithm to the parameters Ω_0, Ω_B, and Δ. After 1600 iterations, we achieve a fidelity of better than 99.9%, or, more precisely, an infidelity $I = (1-F) < 3.8 \times 10^{-4}$. If the experimental precision of the Rabi frequencies and detuning is limited to integer megahertz this infidelity slightly increases to 4.2×10^{-4}. The decrease in infidelity as the algorithm progresses is shown in Fig. 3. Table I shows the final set of parameters that produced the optimized gate. The resulting time-dependent phase accumulations ϕ_{gg} and ϕ_{ge} are shown in Fig. 4. We see that the phase accumulated by the ε_{ge} (ε_{eg}) is exactly zero. This can be understood by calculating Eq. (15) for our set of parameters: since $\delta = 0$, it is straightforward to show that $\varepsilon_{ge}(t) = 0$. The populations of the relevant levels during the gate operation are shown in Fig. 5.

TABLE I. A set of initial parameters that produces a gate with fidelity of around 89%, and the optimized parameters that produce a gate with fidelity better than 99.9%. All values are in units of 2π MHz.

	Ω_0	Ω_B	Δ	δ
Initial	300	300	1000	0
Optimized	304.7	292.6	974.8	0

It might be worrisome that the parameters in Table I do not seem to strongly fulfill the condition $\Omega_R(t), \Omega_R, \delta \ll \Delta$ required for the validity of the adiabatic elimination. We have, however, confirmed that even when we consider the full evolution under $\hat{H}$ in Eq. (2) the population in $|i\rangle$ is heavily suppressed, such that it may be neglected. In what follows, we abandon the effective model given by $\hat{H}_R$ (which provided insight into the gate mechanism) in favor of the full treatment by $\hat{H}$ as given by Eq. (2). This means that we include all four levels of each atom and treat the effective loss by the non-Hermitian term in Eq. (5).

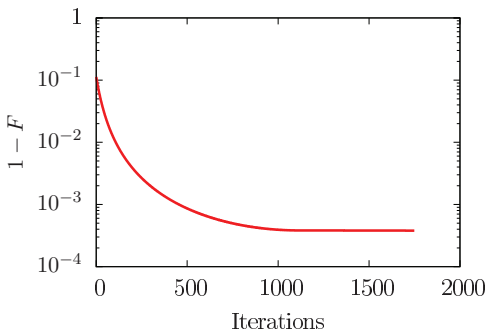

FIG. 3. (Color online) The decrease in infidelity of the quantum gate for the set of initial parameters given in Table I. One sees that the infidelity decreases monotonically until saturating in a local minimum of the optimization. The final achieved infidelity was $1 - F = 3.8 \times 10^{-4}$.

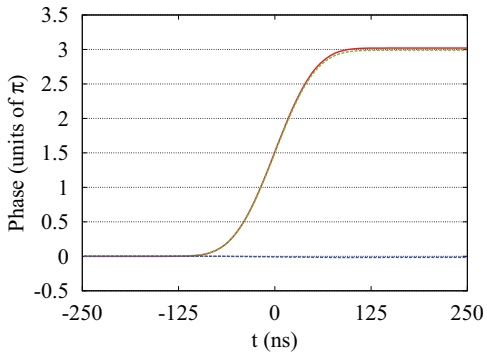

FIG. 4. (Color online) The dashed (green) line is the phase accumulation of the states $|gg\rangle$ (given by ϕ_{gg}), the dotted (blue) line is that of $|ge\rangle$ (given by ϕ_{ge}), and the solid (red) line is the total entanglement phase ϕ, which at the final time reaches 3.0 (note that the dashed green line and the solid red line overlap almost exactly). The parameters used are given in Table I. The time is in units of nanoseconds, and so the duration of the gate is 500 ns.

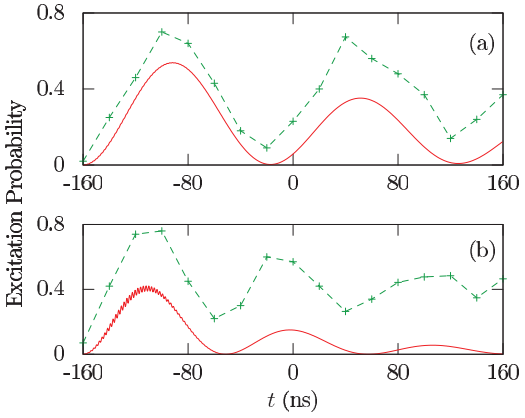

FIG. 6. (Color online) (a) The solid (red) line is the simulated probability to excite $|ge\rangle$ to $|re\rangle$, with the experimental results for the same transition shown as a dashed (green) line. (b) Similarly, the solid (red) line is the simulated probability to excite $|gg\rangle$ to $|\Psi^+\rangle$, with the experimental results for the same transition shown as a dashed (green) line.

IV. EXPERIMENTAL CONSIDERATIONS

A. Level description

We have now demonstrated the optimization method, but we must also consider the experimental conditions which will have an effect on the gate fidelity. We consider the setup given in Ref. [6]. The gate is well suited to this system because we do not require single atoms to be addressable, and the Rydberg blockade is relatively strong. The reason for this is the use of a Förster resonance that exists in ^{87}Rb [20], which comes about due to the quasidegeneracy of the two-atom states $(58d_{3/2}, 58d_{3/2})$ and $(60p_{1/2}, 56f_{5/2})$. This enhances the dipole interaction, leading to an interaction energy $U(r) \propto 1/r^3$.

The choices of states for the levels are $|g\rangle = |5s_{1/2},\ F = 1,\ M_F = 1\rangle$, $|e\rangle = |5s_{1/2},\ F = 2,\ M_F = 2\rangle$, and $|i\rangle = |5p_{1/2},\ F = 2,\ M_F = 2\rangle$, as in Ref. [7].

B. Correspondence to experimental results

As mentioned earlier, we describe the loss from both the intermediate state $|i\rangle$ and the excited Rydberg state $|r\rangle$ phenomenologically through the decay rates γ_i and γ_r, respectively. Examining the literature [9,21], we find for our setup that $\gamma_i = 2\pi \times 5.75$ MHz and $\gamma_r = 2\pi \times 4.8$ kHz.

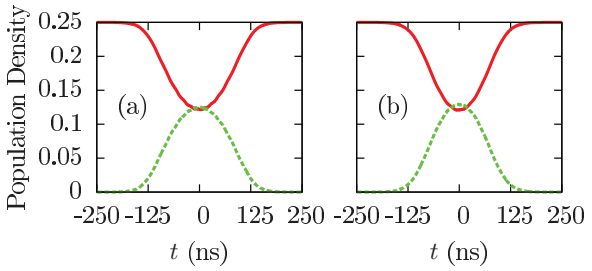

FIG. 5. (Color online) (a) The solid (red) line is the population of the state $|gg\rangle$ and the dashed (green) line is the population of the state $|\Psi^+\rangle$ over the duration of the gate. (b) Similarly to (a), the solid (red) line is the population of the state $|ge\rangle$ and the dashed (green) line is the population of the state $|re\rangle$ over the duration of the gate. The populations of $|eg\rangle$ and $|er\rangle$ are respectively the same.

We have verified that the simulation corresponds to the experimental results from Ref. [6]. Figure 6 shows the agreement between the simulated Rabi oscillations of the $\frac{1}{2}(|er\rangle + |re\rangle)$ state and the $|\Psi^+\rangle$ state. While the fit is not exact, we do reproduce the correct frequency of oscillation, as well as an indication of the typical decay from the intermediate level. We also find a relative difference in frequency of the two oscillations of a factor $\sim\sqrt{2}$, as expected from the theory. The discrepancies between theory and experiment arise from experimental imperfections which are not taken into account in our model, namely laser fluctuations in both power and frequency of the lasers, which lead to some dephasing. Our phenomenological loss model also does not account for the possibility that an atom can decay to $|g\rangle$ from where it may be repumped, which partially accounts for the discrepancy in total population.

C. Typical experimental parameters

While it would be ideal if the gate parameters described in the previous section could be immediately applied in the experiment, the reality is that there are certain experimental limitations that prevent us from doing so. First, the powers of both lasers have certain maximum values: Ω_R has a maximum operating value of 1 GHz, while Ω_B is limited to 120 MHz. Second, we do not have the freedom to modulate the laser power as we like; acousto-optic modulators (AOMs) control the power of the laser beams incident on the atoms, and they have limits on the rate at which the intensity of the beam can be changed. (In any case, since the gate is adiabatic, we expect that the final result will not depend very strongly on the exact shape of the excitation as long as the area of the pulse is preserved.) The "rise time" (the time it takes to increase the laser power from zero to its maximum) is typically in the range 200–400 ns. We take the profile of this rise time to be Gaussian, in agreement with the measured pulse shape on the experiment.

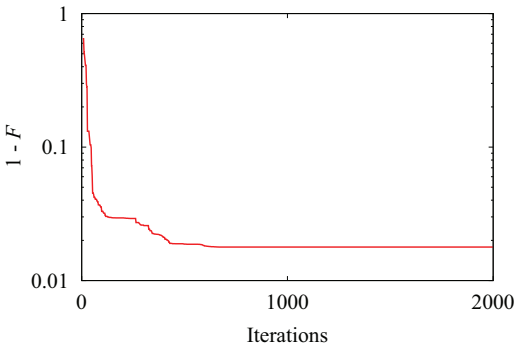

FIG. 7. (Color online) The decrease in infidelity of the quantum gate for the set of initial parameters given in Table II. The stepwise decrease of the current minimum illustrates how restarting the simplex can result in finding another (deeper) local minimum until it reaches the (supposed) global minimum. The final achieved infidelity was $1 - F = 1.8 \times 10^{-2}$.

Finally, due to the separate dipole traps, the minimum distance between the two Rydberg atoms is limited to 3 μm or greater. A final condition is put on the detuning Δ of the red laser: this should be less than 500 MHz due to experimental constraints (although this is not a stringent condition).

There is also an additional probability of loss when an atom is excited to the Rydberg level: when excited, the motional wave packet starts to spread, so that when the dipole trap is reapplied, there is a finite probability that the atom is lost (this is actually used as a method of detection in the experiment). This motivates us to limit the time spent in the Rydberg state.

D. Optimizing the gate for experiment

With these limitations, we now see that the gate parameters from Table I are not feasible in our chosen experimental setup. We must now start with a new set of parameters and run the optimization again to see to what extent the gate is still implementable. Given the discussion above, we are motivated to make the following changes to our parameters.

(a) The gate should be performed as quickly as possible, meaning that the effective Rabi frequency $\tilde{\Omega} \propto \Omega_R, \Omega_B$ should be made large. This implies that we should choose Ω_R and Ω_B close to their maximum values. (This has the additional advantage that we spend less time in excited Rydberg levels, improving the probability of recapture.) Since the constraint is stricter for Ω_B and we want to fully exploit the experimentally feasible maximum power, we set Ω_B to 120 MHz and instead optimize the gate operation time T.

(b) To avoid excitation of the lossy $|i\rangle$ state, we need to keep the red laser far detuned, ideally around 500 MHz. However, as can be seen in Eq. (11), increasing the detuning will reduce the effective Rabi frequency, which makes achieving the gate in a short time more difficult.

TABLE II. A set of initial parameters, within experimental constraints, that produces a gate with fidelity of around 52%, and the optimized parameters that produce a gate with fidelity better than 98%. Rabi frequencies are in units of 2π MHz, time in units of 1 μs.

	Ω_0	T	Δ	δ
Initial	50	1	500	-1
Optimized	129.6	1.1	-703.7	0.1

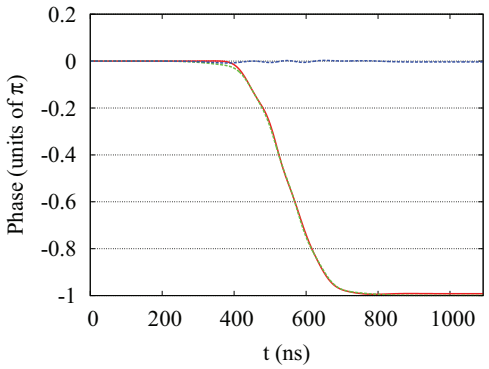

FIG. 8. (Color online) The dashed (green) line is the phase accumulation of the states $|gg\rangle$ (given by ϕ_{gg}), the dotted (blue) line is that of $|ge\rangle$ (given by ϕ_{ge}), and the solid (red) line is the total entanglement phase ϕ, which at the final time reaches -1.0. The parameters used are given in Table II. The time is in units of nanoseconds, and so the duration of the gate is 1.0922 μs.

(c) To make maximum use of the laser power, we change the shape of the pulse from a simple Gaussian to a "flat top," given by

$$\Omega_R = \begin{cases} \Omega_0 \exp\left[-\frac{(t-\tau)^2}{\tau^2/8}\right] & t \leqslant \tau, \\ \Omega_0 \exp\left[-\frac{(t-(T-\tau))^2}{\tau^2/8}\right] & t \geqslant T-\tau, \\ \Omega_0 & \text{otherwise.} \end{cases} \tag{25}$$

Here, the Rabi frequency increases with a Gaussian profile to the maximum Ω_0 in a time τ (the rise time), followed by a period of constant Rabi frequency for a time $T - 2\tau$, and then finally a reduction along a Gaussian profile to zero, again in a time τ. This gives us the freedom to have the laser at full power for the longest time possible, which in turn causes us to accumulate the time-dependent phase more rapidly. It turns out, however, that the best choice for τ is to extend the rise time to $\tau = T/2$, thus choosing a Gaussian profile.

(d) Since the minimum distance between the atoms in the experiment is $r_{\min} = 3.0\,\mu$m, we use this value in what follows to ensure we are as deep in the blockade regime as possible.

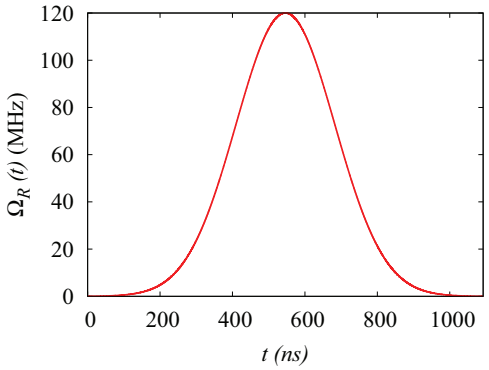

FIG. 9. (Color online) The pulse shape for the Rabi frequency $\Omega_R(t)$ for the parameters in Table II. The shape is a "degenerated flat top," as given in Eq. (25), i.e., a Gaussian profile.

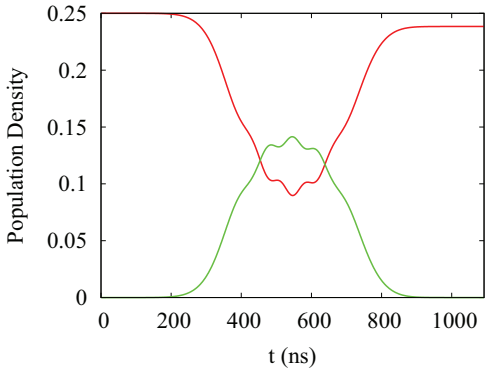

FIG. 10. (Color online) The solid (red) line is the population of the state $|gg\rangle$ and the dashed (green) line is the population of the super-radiant state $|\Psi^+\rangle$ over the duration of the gate.

Based on these considerations, we try the set of parameters given in Table II. This time we use the Nelder-Mead simplex algorithm to optimize the gate parameters since the physics here makes it more challenging to perform a high-fidelity gate and we want to avoid local minima. As before, we can examine the convergence of the optimization (Fig. 7), the accumulation of the entanglement phase (Fig. 8), and the shape of the Rabi frequency $\Omega_R(t)$ (Fig. 9). The final gate fidelity is only around 98%, mainly due to losses, resulting in a final population norm of 0.983. This loss mainly occurs in the time-evolved $|gg\rangle$ state as can be seen in Fig. 10, while the results in Fig. 11 show that there is less loss when time-evolving $|eg\rangle$, since here only one atom is excited. Reducing the precision of Rabi frequencies and detunings to integer megahertz increases the infidelity from 1.8×10^{-2} to 2.2×10^{-2}.

We believe that this result is close to the optimal case for this system and gate implementation given the experimental limitations. Only if we release the constraint on Ω_B can we further improve the fidelity. We have checked that we can cross the 99% fidelity threshold at about $\Omega_B = 200$ MHz which at the moment still needs improvement of experimental equipment.

E. Movement of the atoms in the light field

Until now, we assumed that the atoms were stationary in the dipole traps. In reality, the atoms are Doppler-cooled to around 75 μK. During the laser excitation, the trapping fields are switched off, allowing the atoms to move freely in any direction in the plane perpendicular to the trapping field. The terms $\vartheta_i \equiv \arccos(\mathbf{k} \cdot \mathbf{r}_i) \in [0,\pi]$ from Eq. (10) then produce additional independent phases on each atom. Since we do not know *a priori* in which direction the atoms will move with respect to the light field, the phase difference between the two atoms is essentially random.

Figures 12 and 13 show the effect of this phase on the final fidelity of the gate for the sets of optimal parameters in Tables I and II, respectively. In the first implementation of the gate, we see that the effect of the motional phase on the gate fidelity is, at worst, a drop in infidelity from 1×10^{-4} to 1×10^{-2}. In the second case, the effect is about from 1×10^{-2} to 1×10^{-1}.

To actually perform the gate in practice under these conditions, we would have to cool the atoms much closer to the motional ground state. This would reduce the distance that the atoms move in the light field and, hence, the amount

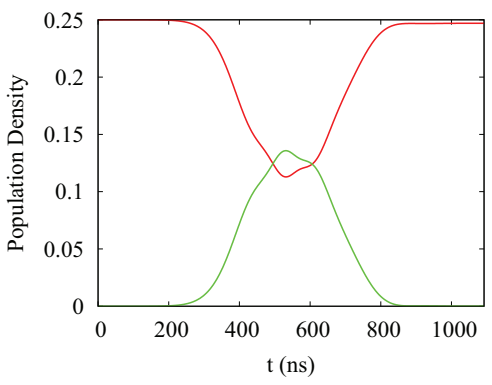

FIG. 11. (Color online) The solid (red) line is the population of the state $|ge\rangle$ and the dashed (green) line is the population of the state $|re\rangle$ over the duration of the gate. The populations of $|eg\rangle$ and $|er\rangle$ are respectively the same.

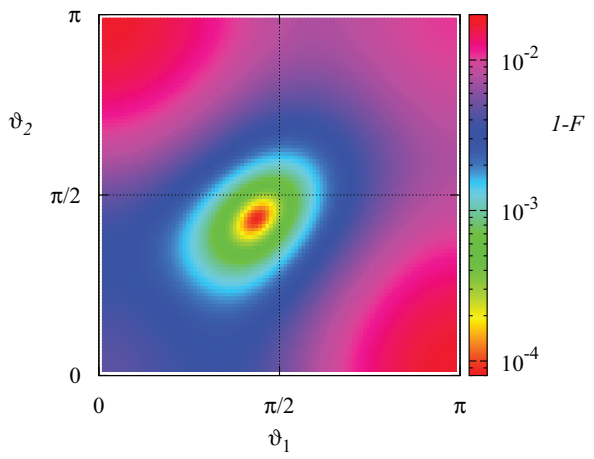

FIG. 12. (Color online) The effect of the motional phases of the atoms on the final gate fidelity for the parameters in Table I. Here, the effect of the motional phases is not too large, since we perform the gate over a very short time and we do not significantly excite the atoms.

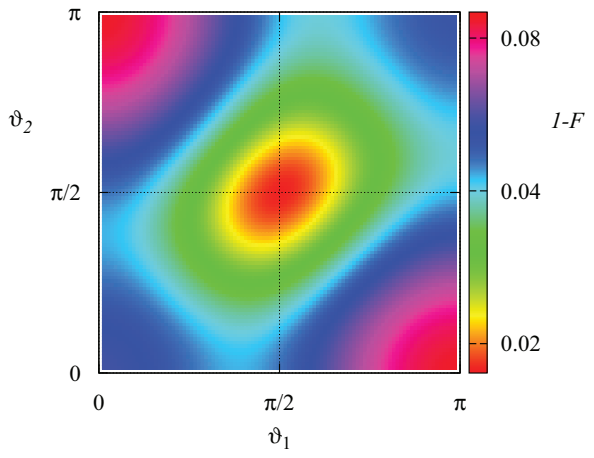

FIG. 13. (Color online) The effect of the motional phases of the atoms on the final gate fidelity for the parameters in Table II. Here, the effect of the motional phases is detrimental to the gate fidelity.

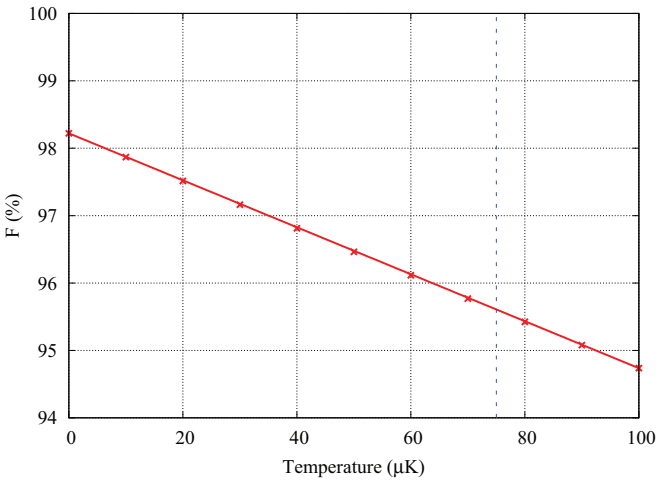

FIG. 14. (Color online) The final fidelity of the gate plotted against the average temperature of the atoms. Each (green) point is an average over 10 000 realizations of ϑ_1 and ϑ_2 chosen randomly in the range $[0,\pi]$. The (red) solid line is a linear fit to the points. The (blue) dashed line shows the current temperature of 75 μK.

of phase that they collect. The dependence of the fidelity on the average temperature of the atoms is given in Fig. 14. Thus reducing the temperature by a factor of around 5 will increase the fidelity to around 97%. This is experimentally realistic as demonstrated in Ref. [22].

V. CONCLUSION

We have investigated the implementation of the Rydberg two-qubit entangling gate from Jaksch *et al.* [4] in the experiment outlined in Ref. [6]. We applied a direct search (gradient descent and Nelder-Mead simplex) control algorithm to find optimal sets of experimental parameters that produced a gate with low loss from the intermediate level while still achieving a fidelity of around 98%. The main source of error was found to be the random phase accumulated by the atoms in the light field.

While the system seems ideally suited for this scheme, the experimental constraints still limit the fidelity of the gate. The most notable source of error comes from the movement of the atoms in the light field, which could be minimized in future experiments by cooling the atoms further. Eliminating this source of error should allow gate fidelities of around 99% which, while not quite good enough to allow quantum computation (even with error correction), would be a significant step forward for the realization of quantum computation with neutral atom systems.

It is worth pointing out that while we investigated the gate scheme of Ref. [4], there are some alternative schemes that could be implemented in our setup, most notably perhaps the scheme of Ref. [5] which uses a STIRAP pulse sequence to excite the atoms and also the individual addressing of atoms as analyzed in detail in Ref. [23]. We have also not investigated allowing the Rabi frequency of the blue laser, Ω_B, to modulate in time which could lead to a more robust gate implementation.

ACKNOWLEDGMENTS

We acknowledge financial support by the EU under Contract No. MRTN-CT-2006-035369 (EMALI) and contracts IP-AQUTE, MALICIA, and SIQS, and from the German SFB TRR21 and QuOReP. We also acknowledge computational resources provided by the BWgrid.

[1] D. Jaksch, H.-J. Briegel, J. I. Cirac, C. W. Gardiner, and P. Zoller, Phys. Rev. Lett. **82**, 1975 (1999).
[2] T. Calarco, H. J. Briegel, D. Jaksch, J. I. Cirac, and P. Zoller, J. Mod. Opt. **47**, 2137 (2000).
[3] M. Saffman, T. G. Walker, and K. Mølmer, Rev. Mod. Phys. **82**, 2313 (2010).
[4] D. Jaksch, J. I. Cirac, P. Zoller, S. L. Rolston, R. Côté, and M. D. Lukin, Phys. Rev. Lett. **85**, 2208 (2000).
[5] D. Møller, L. B. Madsen, and K. Mølmer, Phys. Rev. Lett. **100**, 170504 (2008).
[6] A. Gaëtan, Y. Miroshnychenko, T. Wilk, A. Chotia, M. Viteau, D. Comparat, P. Pillet, A. Browaeys, and P. Grangier, Nat. Phys. **5**, 115 (2009).
[7] T. Wilk, A. Gaëtan, C. Evellin, J. Wolters, Y. Miroshnychenko, P. Grangier, and A. Browaeys, Phys. Rev. Lett. **104**, 010502 (2010).
[8] L. Isenhower, E. Urban, X. L. Zhang, A. T. Gill, T. Henage, T. A. Johnson, T. G. Walker, and M. Saffman, Phys. Rev. Lett. **104**, 010503 (2010).
[9] Y. Miroshnychenko, A. Gaëtan, C. Evellin, P. Grangier, D. Comparat, P. Pillet, T. Wilk, and A. Browaeys, Phys. Rev. A **82**, 013405 (2010).
[10] A. Barenco, D. Deutsch, A. Ekert, and R. Jozsa, Phys. Rev. Lett. **74**, 4083 (1995).
[11] A. Barenco, C. H. Bennett, R. Cleve, D. P. DiVincenzo, N. Margolus, P. Shor, T. Sleator, J. A. Smolin, and H. Weinfurter, Phys. Rev. A **52**, 3457 (1995).
[12] K. Singer, M. Reetz-Lamour, T. Amthor, L. G. Marcassa, and M. Weidemüller, Phys. Rev. Lett. **93**, 163001 (2004).
[13] M. D. Lukin, M. Fleischhauer, R. Cote, L. M. Duan, D. Jaksch, J. I. Cirac, and P. Zoller, Phys. Rev. Lett. **87**, 037901 (2001).
[14] E. Brion, L. H. Pedersen, and K. Mølmer, J. Phys. B **40**, S159 (2007).
[15] M. M. Müller, D. M. Reich, M. Murphy, H. Yuan, J. Vala, K. B. Whaley, T. Calarco, and C. P. Koch, Phys. Rev. A **84**, 042315 (2011).
[16] M. M. Müller, H. R. Haakh, T. Calarco, C. P. Koch, and C. Henkel, Quantum Inf. Process. **10**, 771 (2011).
[17] E. Brion, L. H. Pedersen, and K. Mølmer, J. Phys. A **40**, 1033 (2007).
[18] R. H. Dicke, Phys. Rev. **93**, 99 (1954).
[19] T. Förster, *Modern Quantum Chemistry* (Academic Press, New York, 1996).
[20] T. G. Walker and M. Saffman, J. Phys. B **38**, S309 (2005).
[21] D. A. Steck, http://steck.us/alkalidata
[22] C. Tuchendler, A. M. Lance, A. Browaeys, Y. R. P. Sortais, and P. Grangier, Phys. Rev. A **78**, 033425 (2008).
[23] X. L. Zhang, A. T. Gill, L. Isenhower, T. G. Walker, and M. Saffman, Phys. Rev. A **85**, 042310 (2012).